Journal of the European Ceramic Society **18** (1998) 105–112

PII: S0955-2219(97)00098-8
0955-2219/98/$19.00 + 0.00

Processing and Electrical Conductivity of Pure, Fe- and Cr-substituted $La_{0.9}Sr_{0.1}GaO_3$

R. T. Baker, B. Gharbage and F. M. B. Marques*

Ceramics and Glass Engineering Department, University of Aveiro, 3810 Aveiro, Portugal

(Received 28 January 1997; accepted 18 April 1997)

Abstract

The material $La_{0.9}Sr_{0.1}GaO_3$ and four B-site substituted variants with 5 or 20% Fe or Cr for Ga substitution were prepared by solid state reaction starting from oxide and carbonate precursors. The materials were characterised by scanning electron microscopy (SEM), X-ray diffraction (XRD) and impedance spectroscopy (IS) in air. The sintered samples appeared to have orthorhombic symmetry, had densities higher than 90% of theoretical and had average grain sizes of approx. 1–2·5 μm. However, second phases were detected by XRD and SEM images showed evidence of a liquid, Sr-rich second phase in all samples. The high grain boundary impedances measured were attributed to concentration of this second phase at the grain boundaries. Generally, conductivity increased and activation energy of conduction decreased with increasing degree of substitution. Increasing p*-type electronic conductivity involving Cr^{3+}/Cr^{4+} or Fe^{3+}/Fe^{4+} couples is suggested. Raising the sintering temperature of these materials was shown to increase both their average grain size and their total conductivity.* © *1997 Elsevier Science Limited.*

1 Introduction

$LaGaO_3$-based perovskite materials are of interest because certain compositions exhibit high O^{2-} conductivity at high temperatures. Ishihara *et al.*[1] found that $La_{0.9}X_{0.1}GaO_3$ (X = Sr, Ca or Ba) had a higher conductivity than the undoped material, the maximum being for Sr substitution although Sr solubility was limited to 10%. O^{2-} conductivity was further improved on substitution at the B-site. A maximum value higher than that of yttria stabilised zirconia (YSZ) was reported for the composition $La_{0.9}Sr_{0.1}Ga_{0.8}Mg_{0.2}O_3$, although some *p*-type conductivity was found at high O_2 partial pressures.[2] This was much reduced by the substitution of 10% of the La by Nd. However, this substitution also gave rise to a small decrease in ionic conductivity.[3] These materials may be suitable for application as solid oxide fuel cell (SOFC) electrolytes. However, this would require that the materials had very low electronic conductivity.

The structure of these materials is very tolerant to the incorporation of foreign cations and a large number of cations can be used to partially substitute for either La or Ga. Certain such substitutions may result in modifications to electrical and electrochemical properties which may allow other applications. For example, significant mixed electronic and ionic conductivity may make such materials attractive for use in SOFC electrodes.

In this work, the effect of Fe- and Cr- for Ga substitution on electrical behaviour was investigated. These cations were chosen because Fe^{3+} and Cr^{3+} have similar ionic radii to Ga^{3+} which should allow their successful incorporation into the perovskite matrix. They also have several accessible oxidation states which may lead to the Fe- and Cr-substituted gallates having interesting catalytic properties and/or some electronic conductivity. $La_{0.9}Sr_{0.1}GaO_3$ (to be referred to as LSG) and the partially B-site substituted materials $La_{0.9}Sr_{0.1}Ga_{0.95}Fe_{0.05}O_3$ (5FeLSG), $La_{0.9}Sr_{0.1}Ga_{0.95}Cr_{0.05}O_3$ (5CrLSG), $La_{0.9}Sr_{0.1}Ga_{0.8}Fe_{0.2}O_3$ (20FeLSG) and $La_{0.9}Sr_{0.1}Ga_{0.8}Cr_{0.2}O_3$ (20CrLSG) were studied. The influence of sintering temperature on the morphology and electrical conductivity of these materials was also investigated.

2 Materials Preparation and Experimental Methods

The five sample compositions used in this work were prepared from the La_2O_3, $SrCO_3$, Ga_2O_3 and Fe_2O_3 or Cr_2O_3 powders (Merck). These were wet mixed with ethanol in a ball-mill, calcined at

*To whom correspondence should be addressed.

1100°C for 12 h, ball-milled again, dried and screened to $< 30\,\mu$m. The resulting powder was uniaxially pressed into disks and sintered at 1500°C for 4 h.

Sintered disks of LSG and 5FeLSG were also prepared following the same procedure, but with the sintering step carried out at 1500, 1550 or 1600°C, also for 4 h. SEM images and conductivity measurements were used to study the effect of sintering temperature on morphology and electrical properties.

Characterisation was by XRD (Rigaku diffractometer with Cu source) and SEM (Hitachi S-4100). The sample disks for use in the SEM studies were polished using 7, 3 and 1 μm diamond paste and thermally etched. This was done by heating the disks at 10°C min^{-1} to a set point 50°C lower than the sintering temperature of the material. This temperature was maintained for 15 min before cooling to room temperature at 20°C min^{-1}.

Platinum paste electrodes were painted on each face of the sintered disks and fired at 1000°C. Conductivity measurements were carried out in air between 250 and 1000°C using a four-probe IS technique and a Hewlett Packard 4284A impedance analyser operating over the frequency range 20–10^6 Hz.

3 Results and Discussion

3.1 Structure and microstructure

The XRD spectra of the five materials studied are presented in Fig. 1. All matched with that of orthorhombic $LaGaO_3$ (JCPDS card 24-1102). Table 1 contains the orthorhombic lattice parameters. Cubic structures have been observed for the A- and B-site doped materials, $La_{1-x}Sr_xGa_{1-y}Mg_yO_{2.85}$ ($x = 0.1$–0.2, $y = 0.15$–0.25)[3,4] although orthorhombic symmetry was found for $La_{0.9}Sr_{0.1}GaO_3$.[1,4] Other, small peaks (marked in Fig. 1) were present in positions very similar to those seen by Ishihara *et al.*,[2] one of which they attributed to La_4SrO_7. However, most of these might also be explained by the presence of SrO and possibly Ga_2O_3.

The unit cell volumes and theoretical densities of the five compositions were calculated from the XRD lattice parameters and the molecular masses. Experimental densities were estimated from the dimensions and masses of the sintered pellets and are presented in Table 1. Values were all above 90% of theoretical density, suggesting that the samples were well sintered. Unit cell volume increased slightly with increasing Fe content and decreased with increasing Cr content.

SEM micrographs of samples of all five compositions after polishing and thermal etching showed

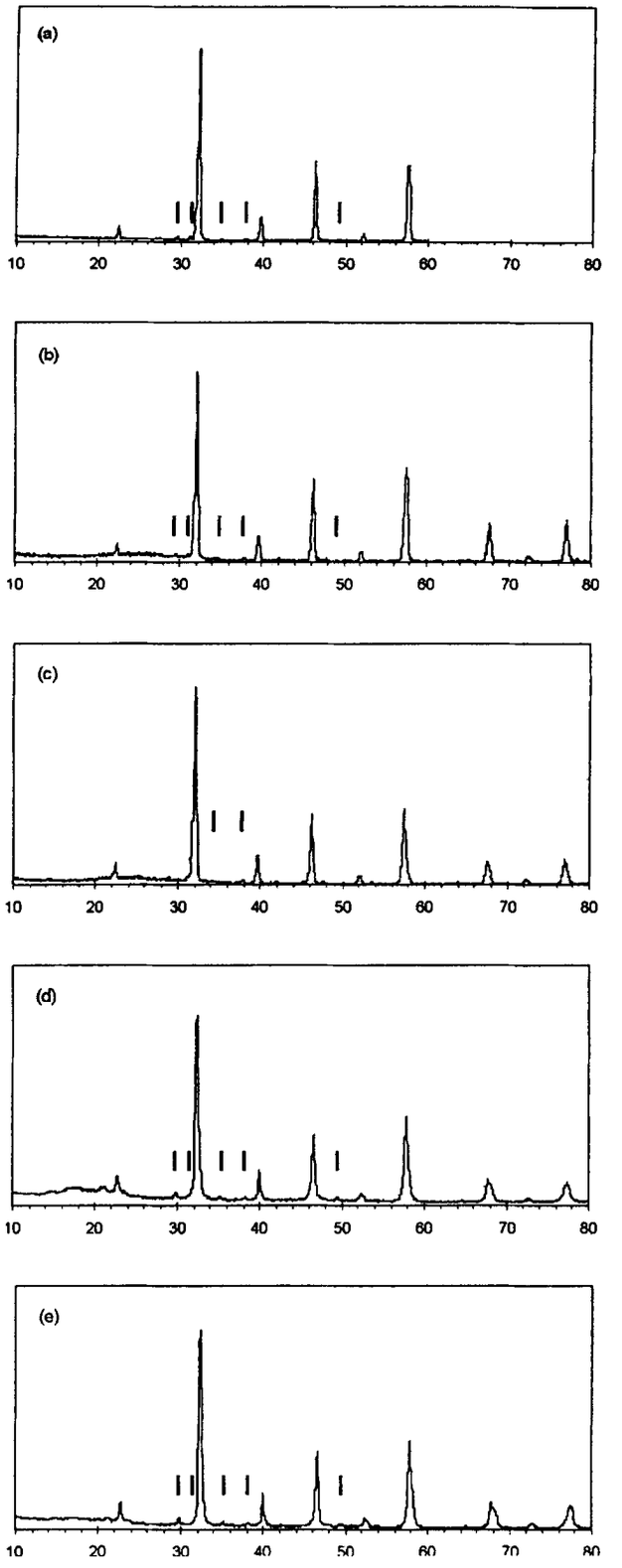

Fig. 1. X-ray diffraction spectra of (a) LSG, (b) 5LSG, (c) 5CrLSG, (d) 20FeLSG and (e) 20CrLSG with unknown peaks marked.

the materials to be dense and to have average grain diameters of around 1 μm when sintered at 1500°C. Examples are given in Fig. 2(a). In all cases, two other phases lying on top of the matrix surface were identified. These were vitreous plates, which had the appearance of a solidified liquid, and needle-shaped crystals [seen in Fig. 2(c)] which

Table 1. Orthorhombic lattice parameters calculated from X-ray data

Material	*LSG*	*5FeLSG*	*20FeLSG*	*5CrLSG*	*20CrLSG*
a (10^{-10} m)	5·515 ±0·015	5·543 ±0·020	5·519 ±0·026	5·515 ±0·001	5·494 ±0·017
b (10^{-10} m)	5·554 ±0·015	5·542 ±0·020	5·574 ±0·027	5·546 ±0·001	5·507 ±0·017
c (10^{-10} m)	7·841 ±0·021	7·829 ±0·028	7·844 0·037	7·798 0·001	7·832 ±0·024
Unit cell volume (10^{-30} m^3)	240·17	240·50	241·30	238·51	236·96
Density (g cm^{-3})	6·39	6·42	6·37	6·64	6·67
Density (% of theoretical)	92	93	93	95	96

appeared to have crystallised from this liquid phase. This attribution was supported by chemical analysis, which revealed their compositions to be practically identical for a given sample. Figure 3(a) shows a plate of the vitreous phase (L) surrounding a pore from which it seems to have emerged. Associated with L are a needle-shaped crystal (N) and what appears to be a crystal (C) partly crystallised from L. The highest surface coverage of the needle shaped crystals and the vitreous plates added together was estimated to be 23%, in the case of a 5FeLSG sample. This estimate was made by superimposing a grid on a low magnification micrograph of one of the samples and calculating the percentage of intersections of the grid which coincided with an example of one of these secondary phases. As it appears that the Sr-rich liquid leaves the bulk of the material at high temperature and concentrates on the surface, the concentration of secondary phases is certain to be much lower within the bulk of the material. Taking into consideration also the small size of XRD peaks attributed to secondary phases, the concentration of secondary phases in the bulk is unlikely to be higher than 5%. These phases contained La, Sr and Ga in all cases and were much richer in Sr than the parent materials matrices, having between 16 and 27 cation% Sr. The averages for the matrices ranged from 2·5 to 4·2 cation%. That is slightly less than the 5 cation% expected for the target composition calculated on the basis of 10% occupancy of the A-site in the perovskite composition ABO_3, where both A and B are cation sites. This implies that Sr diffused out of the grains. Away from the surface, the Sr-rich material probably concentrated at the grain boundaries forming what is likely to be a resistive or poorly-conducting layer.

In the case of 20CrLSG, a further Sr-rich La–Sr–Ga phase, with a different quantitative composition, was found [see Fig. 3(b)], in addition to those already mentioned. This was present as small groups of larger (approx. 3–6 μm) grains (G) dispersed at low concentration within the matrix (M). The concentration of this phase at the surface was estimated as already described and was found to be 4%.

The sintering/reaction mechanism of these materials requires further attention because of the role of microstructure and phase distribution on the electrical properties of these electrolyte materials.

In Fig. 2 SEM images are presented of three samples with the composition LSG and three samples with the composition 5FeLSG which had been sintered at three different temperatures—1500, 1550 and 1600°C—as shown in the figure. All samples were polished and thermally etched. These micrographs were used to calculate the average grain size of the particles in each case. This was done using a digitising pad and pen connected to a computer equipped with appropriate software. A transparency with many straight lines drawn on it was laid over the image. Where a grain on the micrograph was cut by one of these lines, the two points of intersection of the grain boundary with the line were input into the computer using the pen and pad. Between 150 and 450 'grain widths' were entered in this way per micrograph. The straight lines were drawn in such a way as to reduce the effect of any anisotropy in the sample. The results demonstrate the effect on grain size of different sintering temperatures. Mean grain diameters calculated in this way show an increase for both LSG and 5FeLSG compositions as sintering temperature was increased. Mean grain size increased from 1·2 to 1·3 to 1·8 μm for LSG and from 1·2 to 1·3 to 2·5 μm for 5FeLSG, for sintering temperatures of 1500, 1550 and 1600°C, respectively. The grain sizes have a bimodal distribution. This is most clearly seen in the samples sintered at 1600°C where a large number of grains have diameters of around 3 μm and most of the remaining grains have diameters of approx. 1 μm or less. As the sintering temperature decreases, there is a clear decrease in the number of large grains. These changes in mean grain size have a measurable effect on the electrical conductivity of the samples, as described in the next section.

3.2 Electrical characterisation

The impedance spectra taken in air at 300°C of LSG, 5FeLSG and 5CrLSG samples are compared in Fig. 4(a). The traditional designations of bulk and grain boundary arcs will be adopted for simplicity. For these materials and at this temperature, the bulk and grain boundary impedance arcs can be seen clearly. The unusually large grain boundary impedance when compared to the impedance

of the bulk for all materials should be noted. This implies that, although the grains, or bulk, of the material have relatively high conductivities, the boundaries between the grains present unusually high resistance to the flow of ionic current. In high purity sintered disks of common electrolytes such as yttria-stabilised zirconia (YSZ) the grain boundary impedance can be reduced to less than 10–20% of the bulk impedance, even at low temperature. This suggests that the total conductivity

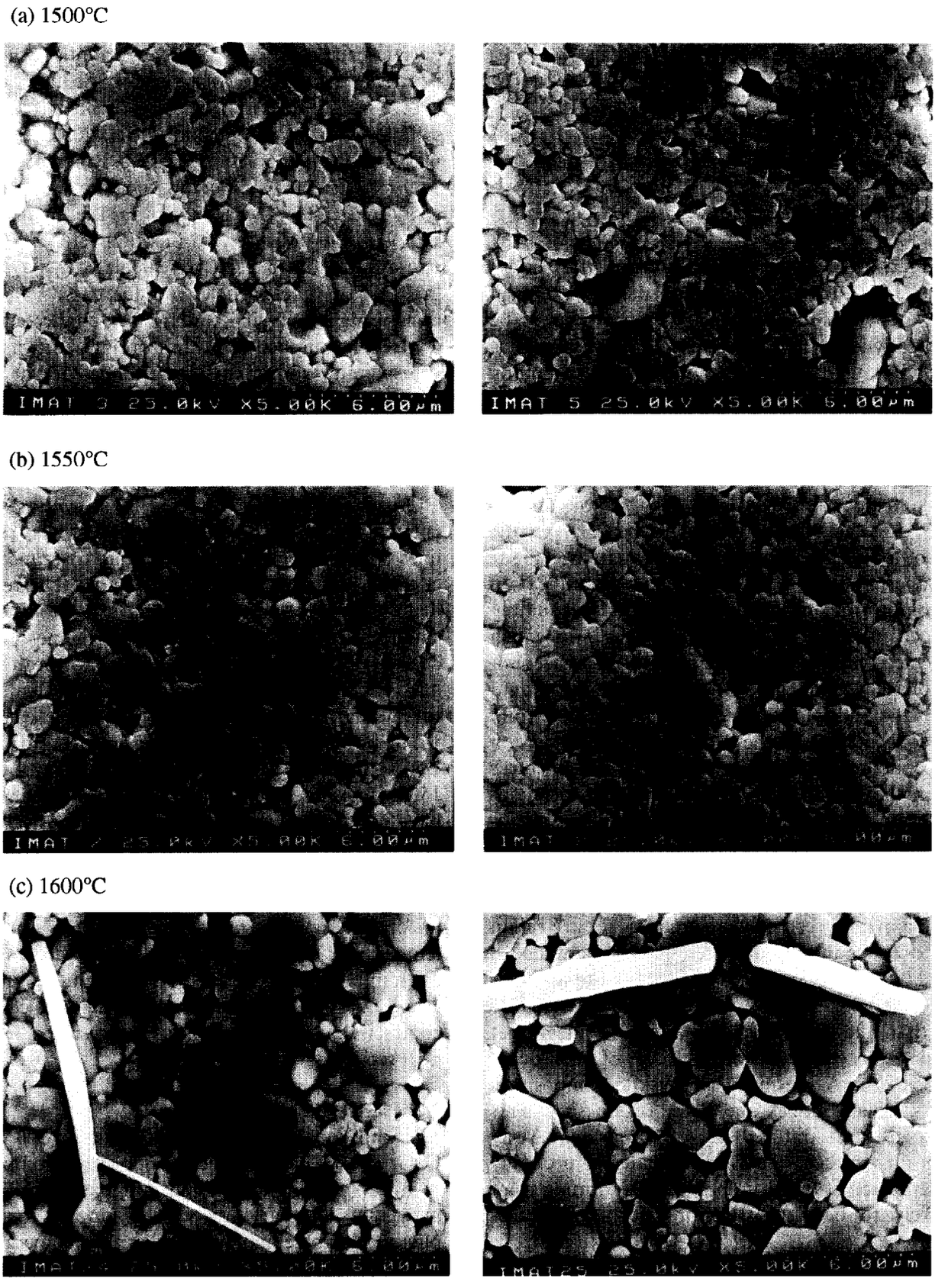

Fig. 2. SEM micrographs of LSG and 5FeLSG prepared at sintering temperatures of (a) 1500°C, (b) 1550°C and 1600°C, as shown.

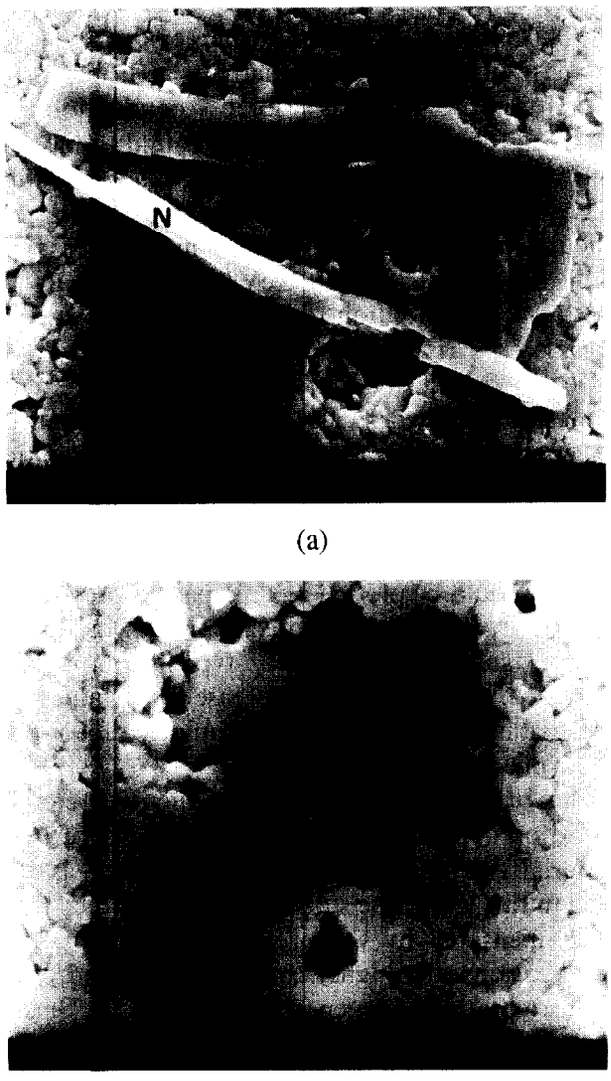

(a)

(b)

Fig. 3. SEM micrographs after polishing and thermal etching showing Sr-rich secondary phases. (a) Vitreous, ex-liquid phase (L), needle-shaped crystal (C) and needle (N) partly crystallised from the vitreous phase. Liquid phase appears to have emerged from pore in surface. (b) 20CrLSG matrix (M) with group of Sr-rich grains (G).

of these materials may be improved by changing the processing conditions in order to increase the average grain size and/or decrease the resistive nature of the grain boundaries themselves. In the existing literature, no information is available on the microstructures or impedance spectra of the material compositions studied in the present contribution. However, Feng and Goodenough[5] present several impedance spectra for the material $La_{0.9}Sr_{0.1}Ga_{0.8}Mg_{0.2}O_3$. The grain boundary arc in these spectra is indeed very small compared to the bulk arc. It is possible that this was due to the extremely high density obtained (99·7% of theoretical), either as a result of the long sintering stage (30 h) or of the presence of Mg. However, the much higher grain boundary impedance measured in this work is likely to be due to the formation of

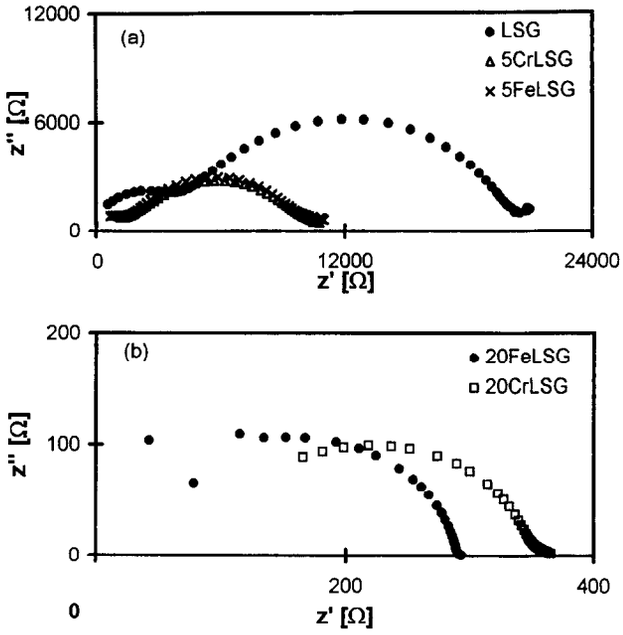

Fig. 4. Impedance spectra in air at 300°C of (a) LSG, 5FeLSG and 5CrLSG and (b) 20FeLSG and 20CrLSG.

a poorly conducting secondary phase at the grain boundary by diffusion of Sr out of the grains, as discussed in the previous section. This process may be suppressed by the presence of Mg at the B-site, giving rise to more conductive grain boundaries.

Figure 4(b) contains the IS spectra, taken under the same conditions, of the more highly substituted samples, 20FeLSG and 20CrLSG. These samples exhibited much higher conductivities (lower impedances) than LSG, 5FeLSG or 5CrLSG, or indeed than YSZ, particularly at such low temperatures. This strongly suggests that these materials gain significant electronic conductivity with Cr or Fe doping, which is dominant at dopant concentrations of 20%. As the conductivity of the materials increases so does the relaxation frequency of the processes related to the semicircular arcs in the IS spectra. In the spectra discussed here (20FeLSG and 20CrLSG), the bulk arc falls outside of the range of the IS spectrometer and for this reason the impedance arcs attributed to bulk and grain boundary impedances are not clearly distinguishable and only the total conductivity values were used for these materials.

Arrhenius plots of the log of total, bulk and grain boundary conductivity for LSG, 5FeLSG and 5CrLSG materials in air are presented in Fig. 5. For 20FeLSG and 20CrLSG only the total conductivity values are given because the individual arcs in these spectra could not be identified, as mentioned above. For the Fe-substituted materials, the total conductivity and the bulk and grain boundary conductivities (at the temperatures where they could be measured, 250–500°C) were superior to those of the undoped material and total

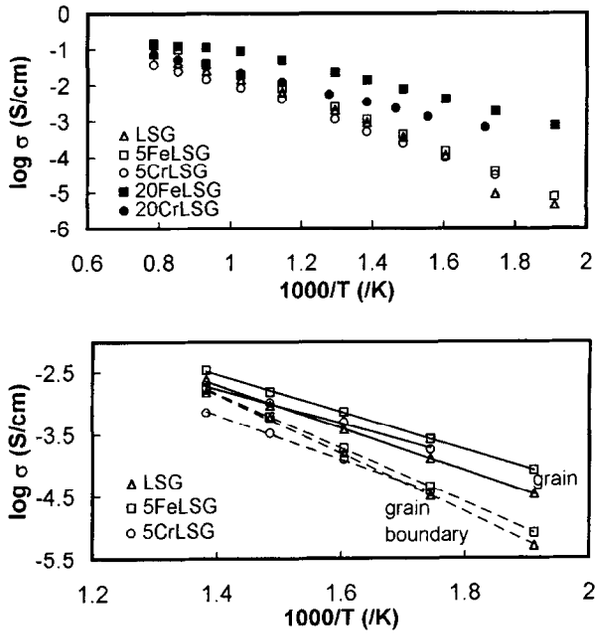

Fig. 5. Arrhenius plots of total conductivity (top) and grain and grain boundary conductivities (bottom) for LSG, 5FeLSG and 5CrLSG.

conductivity increased with increasing degree of substitution. The 5CrLSG material exhibited generally lower total conductivity than the LSG, but was slightly more conductive at the lowest temperatures because of the lower activation energies for both its bulk and grain boundary conductivity. On increasing the extent of substitution, in 20CrLSG, the overall conductivity rose significantly. It could be argued that electronic conductivity increased with Cr content but that there was a competing decrease in ionic conductivity, possibly linked to the decreasing volume of the crystal lattice (Table 1). That is, below the critical Cr concentration required for small polaron hopping, the dominant effect is a decrease in ionic conductivity caused by the reduction in lattice volume. This would explain the conductivity changes on going from 0 to 5 to 20% Cr substitution. Substitution of Fe, on the contrary, caused a modest increase in the lattice volume and total conductivity showed a continuous increase with Fe content.

Table 2 contains activation energy (E_a) values for bulk, grain boundary and overall conductivity in air. All three clearly decrease with increasing B-site substitution. This is further evidence of the increase in electronic conductivity with increasing substitution. Whereas ionic conduction in $La_{0.9}Sr_{0.1}Ga_{0.8}Mg_{0.2}O_3$ has been found to have an activation energy of around 1 eV,[5] the activation energy of electronic conductivity in *p*-type conducting perovskite materials is much lower, typically between 0·5 and 0·1 eV.[6] Therefore, as the electronic contribution to the total conductivity of the material rises, the activation energy would be expected to fall, as is the case here. This is confirmed in other work carried out in this laboratory. By combining data for the *n*- and *p*-type conductivity of these materials obtained from ion blocking experiments with ionic conductivities estimated from IS spectra, the estimated ionic transport number could be plotted against partial pressure of O_2. In air, it was seen to decrease with increasing B-site substitution as *p*-type conductivity increased.[7] Therefore, the decrease in E_a values can be attributed to the increasing influence of *p*-type electronic (low E_a) conduction.

The origin of this *p*-type conductivity can be found on considering the electroneutrality of these materials. In oxidising atmospheres, such as was used in this work, the substitution of La^{3+} by Sr^{2+} is compensated by the promotion of one of the other cations to a higher oxidation state and/or by the formation of oxygen ion vacancies. La, Sr and Ga have stable oxidation states, so the promotion must be from Fe^{3+} to Fe^{4+} and Cr^{3+} to Cr^{4+} for 5FeLSG and 5CrLSG, respectively. Provided that some of the cations remain in the 3+ state, these 3+/4+ couples provide a mechanism for the *p*-type conductivity observed. This behaviour is known for (La,Sr)CrO_3 [8] and for (La,Sr)FeO_3.[9]

As the influence of the grain boundary conductivity (with a relatively high E_a) decreases with temperature, the slopes of the total conductivity Arrhenius curves change gradually with temperature. Therefore, E_a values for total conductivity at both high and low temperature are included in Table 2.

The variation in average grain size seen in Fig. 2 and discussed above is clearly reflected in the conductivity plots of Figs 6 and 7. Over the

Table 2. Activation energies of conduction (eV)

	Material				
Conduction contribution	*LSG*	*5FeLSG*	*20FeLSG*	*5CrLSG*	*20CrLSG*
Bulk (250–500°C)	0·69	0·60	—	0·49	—
Grain boundary (250–500°C)	0·94	0·87	—	0·77	—
Overall (high temperature)	*0·57*	*0·69*	*0·33*	*0·53*	0·38
Overall (250–1000°C)	*0·76*	*0·75*	*0·48*	*0·64*	0·42
Overall (low temperature)	*0·93*	*0·82*	*0·53*	*0·68*	0·42

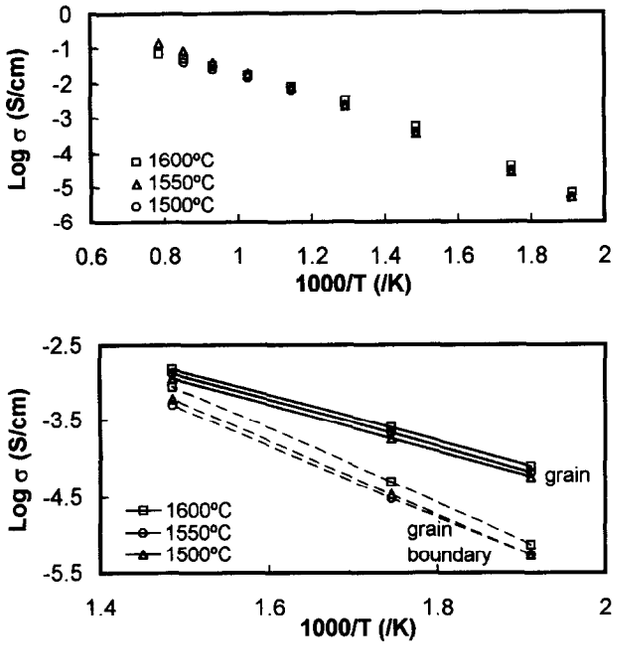

Fig. 6. Arrhenius plots of total conductivity (top) and grain and grain boundary conductivities (bottom) for LSG samples sintered at the temperatures shown.

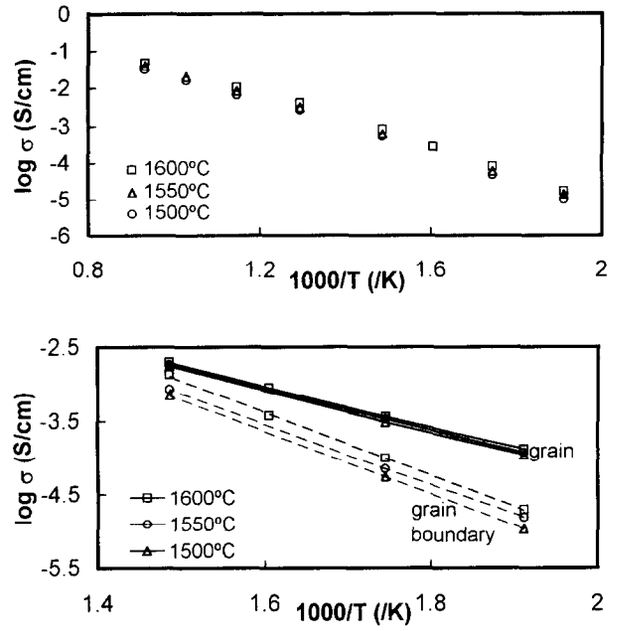

Fig. 7. Arrhenius plots of total conductivity (top) and grain and grain boundary conductivities (bottom) for 5LSG samples sintered at the temperatures shown.

temperature range at which they could be determined, the grain boundary conductivities for both compositions increased with increasing sintering temperature causing the overall conductivities to increase according to the same trend. This effect can be attributed to the reduction in the number of grain boundaries crossed by the ionic current. It is unlikely to be an effect of reduction of porosity with increasing sintering temperature as the materials already had little porosity (see density values

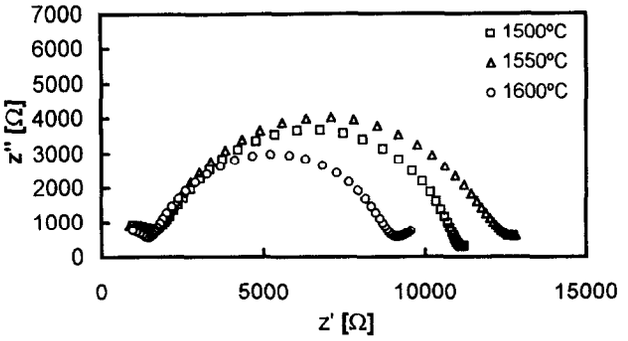

Fig. 8. Impedance spectra taken at 300°C in air of LSG samples sintered at 1500, 1550 or 1600°C.

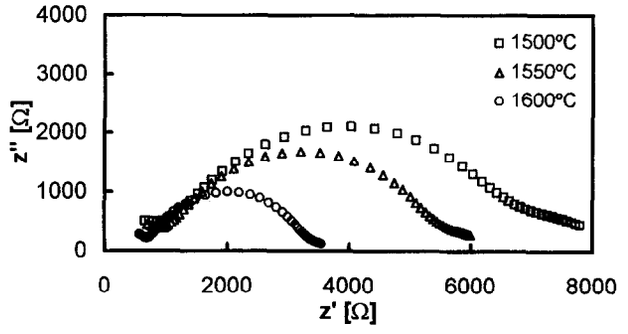

Fig. 9. Impedance spectra taken at 300°C in air of 5FeLSG samples sintered at 1500, 1550 or 1600°C.

in Table 1) after sintering at the lowest temperature used here, 1500°C. The only exception to this trend was for LSG (Fig. 6) sintered at 1500°C whose conductivity was slightly higher than for that sintered at 1550°C. However, the difference in grain size distribution in these two cases is small.

The grain (or bulk) conductivities also increased with sintering temperature although the values were very close together, confirming that the changes are due essentially to changes in grain size distribution rather than in the chemical composition of the material itself.

Both the change in grain boundary impedance and the relative constancy of the bulk impedance can be seen in Figs 8 and 9, where the IS spectra taken at 300°C in air are compared for LSG and 5FeLSG, respectively. Although the spectra are not corrected with respect to the geometries of the different samples, these geometries were very similar.

4 Conclusions

In all of the material compositions studied, second phases similar to those reported[2] were detected by XRD and SEM images showed evidence of a vitreous, Sr-rich second phase in all samples. The grain boundary arc in IS spectra was very large

compared to those of other electrolyte materials, such as YSZ, and $La_{0.9}Sr_{0.1}Ga_{0.8}Mg_{0.2}O_3$ as reported by Feng and Goodenough.[5] It is suggested that this resulted from the presence of a poorly conducting layer of this Sr-rich phase at the grain boundaries.

Compositional modifications in the B-site are likely to give rise to a series of materials with properties ranging from pure electrolyte behaviour to dominant electronic conductivity. Activation energies of conduction decreased, and conductivity values showed a general increase, with increasing degree of substitution, in air. This suggests increasing electronic (*p*-type) conductivity with increasing Fe or Cr for Ga substitution. In air, the conduction mechanism is likely to involve the redox couples Fe^{3+}/Fe^{4+} and Cr^{3+}/Cr^{4+}.

In the samples containing Cr, some evidence exists for a competing increase in electronic conductivity and decrease in ionic conductivity, possibly linked to decreasing unit cell volume, with increasing Cr content.

Improved processing routes are required to produce single phase materials and/or optimised microstructures. Increasing sintering temperature caused an increase in average grain size and in conductivity for the compositions LSG and 5FeLSG.

References

1. Ishihara, T., Matsuda, H. and Takita, Y., Doped $LaGaO_3$ perovskite type oxide as a new oxide ionic conductor. *Journal of the American Chemical Society*, 1994, **116**, 3801–3803.
2. Ishihara, T., Matsuda, H. and Takita, Y., Effect of rare earth cations doped for la site on the oxide ionic conductivity of LaGa O_3-based perovskite type oxide. *Solid State Ionics*, 1995, **79**, 147–151.
3. Ishihara, T., Hiei, Y. and Takita, Y., Oxidative reforming with methane using solid oxide fuel cell with $LaGaO_3$-based electrolyte. *Solid State Ionics*, 1995, **79**, 371–375.
4. Huang, P. and Petric, A., Superior oxygen ion conductivity of lanthanum gallate doped with strontium and magnesium. *Journal of the Electrochemical Society*, 1996, **143**(5), 1644–1648.
5. Feng, M. and Goodenough, J. B., A superior oxide-ion electrolyte. *European Journal of Solid State and Inorganic Chemistry*, 1994, **31**, 663–672.
6. Subba Rao, G. V., Wanklyn, B. M. and Rao, C. N. R., Electrical transport in rare earth ortho-chromites, -manganites and -ferrites. *Journal of Physics and Chemistry of Solids*, 1971, **32**, 345–358.
7. Baker, R. T., Gharbage, B. and Marques, F. M. B., Ionic and electronic conduction in Fe and Cr d Doped (La, Sr)GaO_3. *Journal of the Electrochemical Society*, 1997 (in press).
8. Mizusaki, J., Yamaouchi, S., Fueki, K. and Ishikawa, A., Nonstoichiometry of the perovskite-type oxide $La_{1-x}Sr_x$ $CrO_{3-\delta}$. *Solid State Ionics*, 1984, **12**, 119–124.
9. Mizusaki, J., Sasamoto, T., Cannon, W. R. and Bowen, H. K., Electronic conductivity, Seebeck coefficient and defect structure of $La_{1-x}Sr_xFeO_3$ (x = 0·1, 0·25). *Journal of the American Ceramic Society*, 1983, **66**(4), 247–252.